Dressed Collective Qubit States and the Tavis-Cummings Model in Circuit QED

J. M. Fink,[1] R. Bianchetti,[1] M. Baur,[1] M. Göppl,[1] L. Steffen,[1] S. Filipp,[1] P. J. Leek,[1] A. Blais,[2] and A. Wallraff[1]

[1]*Department of Physics, ETH Zurich, CH-8093, Zurich, Switzerland*
[2]*Département de Physique, Université de Sherbrooke, Sherbrooke, Québec J1K 2R1, Canada*
(Received 20 April 2009; published 17 August 2009)

We present an ideal realization of the Tavis-Cummings model in the absence of atom number and coupling fluctuations by embedding a discrete number of fully controllable superconducting qubits at fixed positions into a transmission line resonator. Measuring the vacuum Rabi mode splitting with one, two, and three qubits strongly coupled to the cavity field, we explore both bright and dark dressed collective multiqubit states and observe the discrete $\sqrt{N}$ scaling of the collective dipole coupling strength. Our experiments demonstrate a novel approach to explore collective states, such as the W state, in a fully globally and locally controllable quantum system. Our scalable approach is interesting for solid-state quantum information processing and for fundamental multiatom quantum optics experiments with fixed atom numbers.

　　　PACS numbers: 42.50.Ct, 03.67.Lx, 42.50.Pq, 85.35.Gv

In the early 1950s, Dicke realized that under certain conditions, a gas of radiating molecules shows the collective behavior of a single quantum system [1]. The idealized situation in which N two-level systems with identical dipole coupling are resonantly interacting with a single mode of the electromagnetic field was analyzed by Tavis and Cummings [2]. This model predicts the collective N-atom interaction strength to be $G_N = g_j\sqrt{N}$, where g_j is the dipole coupling strength of each individual atom j. In fact, in first cavity QED experiments, the normal mode splitting, observable in the cavity transmission spectrum [3,4], was demonstrated with on average $\bar{N} > 1$ atoms in optical [5,6] and microwave [7] cavities to overcome the relatively weak dipole coupling g_j. The $\sqrt{N}$ scaling has been observed in the regime of a small mean number of atoms $\bar{N}$ with dilute atomic beams [7–9] and fountains [10] crossing a high-finesse cavity. In these experiments, spatial variations of the atom positions and Poissonian fluctuations in the atom number inherent to an atomic beam [4,8,11] are unavoidable. In a different limit where the cavity was populated with a very large number of ultracold ^{87}Rb atoms [12] and more recently with Bose-Einstein condensates [13,14], the $\sqrt{N}$ nonlinearity was also demonstrated. However, the number of interacting atoms is typically only known to about ~10% [13].

Here, we present an experiment in which the Tavis-Cummings model is studied for a discrete set of fully controllable artificial atoms at fixed positions and with virtually identical couplings to a resonant cavity mode. The investigated situation is sketched in Fig. 1(a), depicting an optical analog where three two-state atoms are deterministically positioned at electric field antinodes of a cavity mode where the coupling is maximum. In our circuit QED [15,16] realization of this configuration [Fig. 1(b)], three transmon-type [17] superconducting qubits are embedded in a microwave resonator which contains a quantized radiation field. The cavity is realized as a

coplanar waveguide resonator with a first harmonic full wavelength resonance frequency of $\omega_r/2\pi = 6.729$ GHz and a photon decay rate of $\kappa/2\pi = 6.8$ MHz. The qubits are positioned at the antinodes of the first harmonic standing wave electric field. The transition frequency between ground $|g\rangle$ and first excited state $|e\rangle$ of qubit j, approximately given by $\omega_j \approx \sqrt{8E_{C_j}E_{J_j}(\Phi_j)}/\hbar - E_{C_j}/\hbar$, is controllable through the flux-dependent Josephson energy $E_{J_j}(\Phi_j) = E_{J\max_j}|\cos(\pi\Phi_j/\Phi_0)|$ [17]. Here, E_{C_j} is the single electron charging energy, $E_{J\max_j}$ the maximum Josephson energy at flux $\Phi_j = 0$, and Φ_0 the magnetic flux quantum. Independent flux control of each qubit is achieved by applying magnetic fields with three external miniature current biased coils [Fig. 2(a)] where we take into account all cross couplings by inverting the full cou-
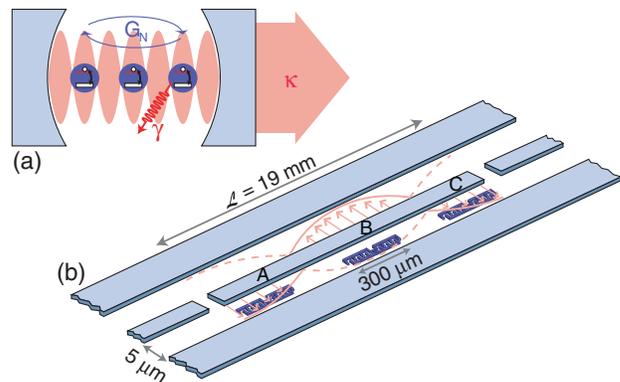

FIG. 1 (color online). Schematic of the experimental setup. (a) Optical analog. Three two-state atoms are identically coupled to a cavity mode with photon decay rate κ, atomic energy relaxation rate γ, and collective coupling strength G_N. (b) Schematic of the investigated system. The coplanar waveguide resonator is shown in gray (light blue), the transmon qubits A, B, and C in dark gray (violet) and the first harmonic of the standing wave electric field in light gray (red).

pling matrix. Optical images of the investigated sample are
depicted in Figs. 2(b) and 2(c). The resonator was fabri-
cated employing optical lithography and aluminum evapo-
ration techniques on a sapphire substrate. All qubits were
fabricated with electron beam lithography and standard
Al/AlO$_x$/Al shadow evaporation techniques. Table I states
the individual qubit parameters obtained from spectro-
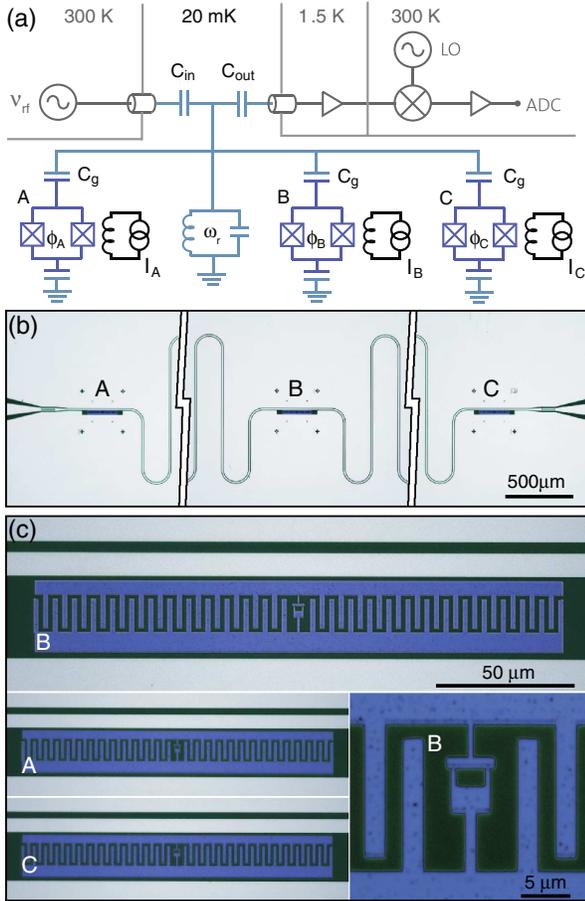scopic measurements.

FIG. 2 (color online). Circuit diagram and false color optical
images of the sample. (a) Simplified electrical circuit diagram of
the experimental setup. The waveguide resonator operated at a
temperature of 20 mK, indicated as LC oscillator with frequency
ω_r, is coupled to input and output leads with the capacitors C_{in}
and C_{out}. Qubits A, B, and C are controlled with external current
biased coils ($I_{A,B,C}$) and coupled to the resonator via identical
capacitors C_g. A transmission measurement is performed by
applying a measurement tone ν_{rf} to the input port of the
resonator, amplifying the transmitted signal and digitizing it
with an analog-to-digital converter (ADC) after down conversion
with a local oscillator (LO) in a heterodyne detection scheme.
(b) The coplanar microwave resonator is shown truncated in gray
(light blue) on the substrate in black (dark green) and the
locations of qubits A, B, and C are indicated. (c) Top, magnified
view of transmon qubit B shown in dark gray (violet) embedded
between ground plane and center conductor of the resonator.
Bottom left, qubits A and C, of same dimensions as qubit B, are
shown at reduced scale. Bottom right, magnified view of SQUID
loop of qubit B.

The physics of our system is described by the Tavis-
Cummings Hamiltonian [2]

$$\hat{\mathcal{H}}_{TC} = \hbar\omega_r \hat{a}^\dagger \hat{a} + \sum_j \left(\frac{\hbar}{2}\omega_j \hat{\sigma}_j^z + \hbar g_j(\hat{a}^\dagger \hat{\sigma}_j^- + \hat{\sigma}_j^+ \hat{a}) \right), \quad (1)$$

where g_j is the coupling strength between the field and
qubit j. $\hat{a}^\dagger$ and $\hat{a}$ are the creation and annihilation operators
of the field, $\hat{\sigma}_j^+$ and $\hat{\sigma}_j^-$ are the corresponding operators
acting on the qubit j, and $\hat{\sigma}_j^z$ is a Pauli operator. The ground
state $|g, g, g\rangle \otimes |0\rangle$ of the three-qubit plus cavity system is
prepared by cooling the microchip to a temperature of
20 mK in a dilution refrigerator.

First, we investigate the resonant coupling of the $|g\rangle$ to
$|e\rangle$ transition of qubit A to the first harmonic mode of the
resonator. We measure the anticrossing between qubit A
(ν_A) and the cavity (ν_r) by populating the resonator with
much less than a photon on average. We record the result-
ing transmission spectrum T versus magnetic flux Φ_A
controlled detuning of qubit A [Fig. 3(a)]. Qubits B and
C remain maximally detuned from the resonator at $\Phi_B = \Phi_C = \Phi_0/2$ where they do not affect the measurement. At
finite detuning [left-hand side of Fig. 3(a)], we observe a
shift of the resonator spectrum which increases with de-
creasing detuning due to the dispersive interaction with
qubit A.

On resonance ($\omega_j = \omega_r$) and in the presence of just one
two-level system ($N = 1$), Eq. (1) reduces to the Jaynes-
Cummings Hamiltonian [18]. The eigenstates $|N, n\pm\rangle$ of
this system in the presence of a single excitation $n = 1$ are
the symmetric and antisymmetric qubit-photon superposi-
tions $|1, 1\pm\rangle = 1/\sqrt{2}(|g, 1\rangle \pm |e, 0\rangle)$ [Fig. 4(a)] where the
excitation is equally shared between qubit and photon.
Accordingly, we observe a clean vacuum Rabi mode split-
ting spectrum formed by the states $|1, 1\pm\rangle$ [Fig. 3(b)].
From analogous measurements performed on qubits B
and C (not shown), we obtain the single qubit coupling
constants g_j listed in Table I. The coupling strengths are
virtually identical with a scatter of only a few MHz. The
strong coupling of an individual photon and an individual
two-level system has been observed in a wealth of different
realizations of cavity QED both spectroscopically
[15,19,20] and in time-resolved experiments [21,22]. The
regime of multiple excitations n which proves field quan-
tization in these systems has been reported both in the

TABLE I. Qubit and qubit-resonator coupling parameters. The
single electron charging energy E_{C_j}, the maximum Josephson
energy $E_{J\max_j}$ extracted from spectroscopic measurements, and
the coupling strengths g_j obtained from resonator transmission
measurements for qubits A, B, and C.

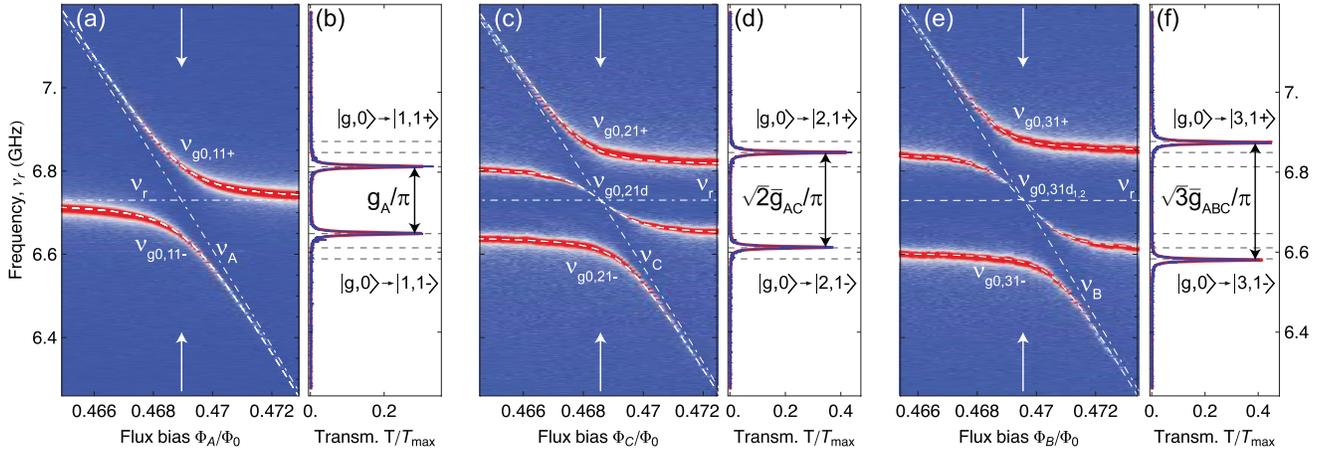| Qubit j	E_{C_j}/h (MHz)	$E_{J\max_j}/h$ (GHz)	$g_j/2\pi$ (MHz)
A	283	224	83.7
B	287	226	−85.7
C	294	214	85.1

FIG. 3 (color online). Vacuum Rabi mode splitting with one, two, and three qubits. (a) Measured resonator transmission spectrum T [gray (blue) corresponds to low and dark gray (red) to high transmission] versus normalized external flux bias Φ_A/Φ_0 of qubit A. Dash-dotted white lines indicate bare resonator ν_r and qubit ν_A frequencies and dashed white lines are calculated transition frequencies $\nu_{g0,Nn\pm}$ between $|g,0\rangle$ and $|N,n\pm\rangle$. (b) Resonator transmission $T/T_{\max}$ at degeneracy normalized to the maximum resonator transmission $T_{\max}$ measured at $\Phi_{A,B,C} = \Phi_0/2$ (not shown), as indicated with arrows in (a). Dark gray (red) line is a fit to two Lorentzians. (c) Resonator transmission spectrum $T/T_{\max}$ versus external flux bias Φ_C/Φ_0 of qubit C with qubit A degenerate with the resonator ($\nu_A = \nu_r$). (d) Transmission spectrum $T/T_{\max}$ at flux as indicated in (c). (e) Transmission spectrum versus flux Φ_B/Φ_0 with both qubits A and C at degeneracy ($\nu_A = \nu_C = \nu_r$). The white dashed line at frequency $\nu_{g0,31d_{1,2}} = \nu_r$ indicates the dark state occurring at degeneracy. (f) Transmission spectrum $T/T_{\max}$ at flux as indicated in (e).

time-resolved results cited above and, more recently, also in spectroscopic measurements [23–25].

In a next step, we maintain qubit A at degeneracy ($\nu_A = \nu_r$), where we observed the one-photon one-qubit doublet [see left of Fig. 3(c)]. Qubit B remains far detuned ($\Phi_B = \Phi_0/2$) for the entire measurement. Qubit C is then tuned through the already coupled states from lower to higher values of flux Φ_C. In this case, the doublet states $|1, 1\pm\rangle$ of qubit A are found to be dispersively shifted due to non-resonant interaction with qubit C [Fig. 3(c)]. When both qubits and the resonator are exactly in resonance, the transmission spectrum T [Fig. 3(d)] shows only two distinct maxima corresponding to the doublet $|2, 1\pm\rangle = 1/\sqrt{2}|g, g\rangle \otimes |1\rangle \pm 1/2(|e, g\rangle + |g, e\rangle) \otimes |0\rangle$ with eigenenergies $\hbar(\omega_r \pm G_2)$. Here, a single excitation is shared between one photon, with probability $1/2$, and two qubits, with probability $1/4$ each [Fig. 4(b)]. Both states have a photonic component and can be excited from the ground state $|g, g, g\rangle \otimes |0\rangle$ by irradiating the cavity with light. These are thus referred to as bright states. In general, we expect $N + n = 3$ eigenstates for two qubits and one photon. The third state $|2, 1d\rangle = 1/\sqrt{2}(|e, g\rangle - |g, e\rangle) \otimes |0\rangle$ with energy $\hbar\omega_r$ at degeneracy has no matrix element with a cavity excitation and is referred to as a dark state. Accordingly, we observe no visible population in the transmission spectrum at frequency ν_r at degeneracy. In this regime, the two qubits behave like one effective spin with the predicted [26] coupling strength $G_2 = \sqrt{2}\bar{g}_{AC}$ with $\bar{g}_{AC} = \sqrt{1/2(g_A^2 + g_C^2)}$, which is indicated by dashed black lines in Fig. 3(d). This prediction is in very good agreement with our measurement.

Following the same procedure, we then flux tune qubit B through the already resonantly coupled states of qubits A, C, and the cavity ($\nu_A = \nu_C = \nu_r$) [Fig. 3(e)]. We observe the energies of three out of $N + n = 4$ eigenstates, the fourth one being dark, for a range of flux values Φ_B. Starting with the dark state $|2, 1d\rangle$ at frequency ν_r and the doublet $|2, 1\pm\rangle$ [left part of Fig. 3(e)], the presence of qubit B dresses these states and shifts the doublet $|2, 1\pm\rangle$ down in frequency. Again, one of these states turns dark as it approaches degeneracy where it is entirely mixed with qubit B. At degeneracy, we identify two bright doublet states $|3, 1\pm\rangle = 1/\sqrt{2}|g, g, g\rangle \otimes |1\rangle \pm 1/\sqrt{6}(|e, g, g\rangle - |g, e, g\rangle + |g, g, e\rangle) \otimes |0\rangle$ [Fig. 4(c)]. The part of the states
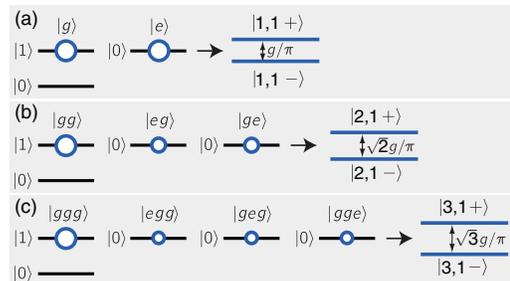

FIG. 4 (color online). Level diagram representing the total energy of (a) one, (b) two, and (c) three qubits resonantly coupled to a single photon. Bare energy levels of the qubits $|g\rangle$, $|e\rangle$ and the cavity $|0\rangle$, $|1\rangle$ are shown in black. The bright dressed energy levels $|N, n\pm\rangle$, with N qubits, n excitations, and $\pm$ indicating the symmetry of the state, are shown as dark gray (blue) lines. The areas of the circles indicate the relative population of the bare states in the eigenstates $|N, n\pm\rangle$.
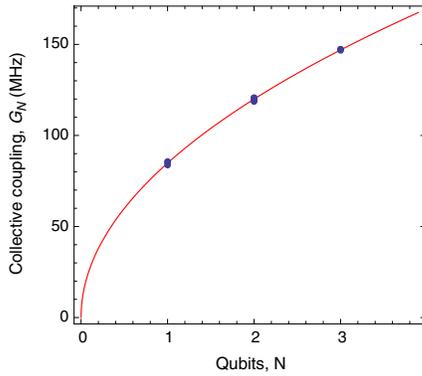
FIG. 5 (color online).   Scaling of the collective dipole coupling strength. Measured coupling constants (dots) extracted from Fig. 3 and nine similar data sets and theoretical scaling (line).

$|3, 1\pm\rangle$ carrying the atomic excitation is a so-called W state, in which a single excitation is equally shared among all N qubits [27]. Both $|3, 1\pm\rangle$ states are clearly visible in the transmission spectrum shown in Fig. 3(f).

In addition, there are two dark states $|3, 1d_1\rangle = 1/\sqrt{2}(|e, g, g\rangle - |g, g, e\rangle) \otimes |0\rangle$ and $|3, 1d_2\rangle = 1/\sqrt{2}(|g, e, g\rangle + |g, g, e\rangle) \otimes |0\rangle$ which do not lead to resonances in the transmission spectrum at degeneracy. In general, all $N + n - 2$ dark states are degenerate at energy $\hbar\omega_r$. The symmetries of the dressed three-qubit states are determined by the signs of the coupling constants $g_A \approx -g_B \approx g_C$. While our measurement is not sensitive to the sign of coupling, it is a simple consequence of the phase shift of the electric field mode by π between the ends and the center of the resonator. Again, the observed transmission peak frequencies are in agreement with the calculated splitting of the doublet $G_3 = \sqrt{3}\bar{g}_{ABC}$ [dashed black lines in Fig. 3(f)]. Also at finite detunings, the measured energies of all bright states are in excellent agreement with the predictions based on the Tavis-Cummings model [dashed white lines in Figs. 3(a), 3(c), and 3(e)] using the measured qubit and resonator parameters. We have also performed analogous measurements of all 12 one-, two-, and three-qubit anticrossings (9 are not shown) and find equally good agreement.

In Fig. 5, all 12 measured coupling strengths (dots) for one, two, and three qubits at degeneracy are plotted vs N. Excellent agreement with the expected collective interaction strength $G_N = \sqrt{N}\bar{g}_{ABC}$ (line) is found without any fit parameters and $\bar{g}_{ABC} = 84.8$ MHz.

Our spectroscopic measurements clearly demonstrate the collective interaction of a discrete number of quantum two-state systems mediated by an individual photon. All results are in good agreement with the predictions of the basic Tavis-Cummings model in the absence of any number, position or coupling fluctuations. The presented approach may enable novel investigations of superradiant and subradiant states of artificial atoms. Flux tuning on nanosecond time scales should furthermore allow the controlled

generation of Dicke states [28,29] and fast entanglement generation via collective interactions [30,31], not relying on individual qubit operations. This could be used for quantum state engineering and an implementation of Heisenberg limited spectroscopy [32] in the solid state.

[1] R. H. Dicke, Phys. Rev. **93**, 99 (1954).
[2] M. Tavis and F. W. Cummings, Phys. Rev. **170**, 379 (1968).
[3] G. S. Agarwal, Phys. Rev. Lett. **53**, 1732 (1984).
[4] S. Leslie, N. Shenvi, K. R. Brown, D. M. Stamper-Kurn, and K. B. Whaley, Phys. Rev. A **69**, 043805 (2004).
[5] M. G. Raizen, R. J. Thompson, R. J. Brecha, H. J. Kimble, and H. J. Carmichael, Phys. Rev. Lett. **63**, 240 (1989).
[6] Y. Zhu *et al.*, Phys. Rev. Lett. **64**, 2499 (1990).
[7] F. Bernardot, P. Nussenzveig, M. Brune, J. M. Raimond, and S. Haroche, Europhys. Lett. **17**, 33 (1992).
[8] J. J. Childs, K. An, M. S. Otteson, R. R. Dasari, and M. S. Feld, Phys. Rev. Lett. **77**, 2901 (1996).
[9] R. J. Thompson, Q. A. Turchette, O. Carnal, and H. J. Kimble, Phys. Rev. A **57**, 3084 (1998).
[10] P. Münstermann, T. Fischer, P. Maunz, P. W. H. Pinkse, and G. Rempe, Phys. Rev. Lett. **84**, 4068 (2000).
[11] H. J. Carmichael and B. C. Sanders, Phys. Rev. A **60**, 2497 (1999).
[12] A. K. Tuchman *et al.*, Phys. Rev. A **74**, 053821 (2006).
[13] F. Brennecke *et al.*, Nature (London) **450**, 268 (2007).
[14] Y. Colombe *et al.*, Nature (London) **450**, 272 (2007).
[15] A. Wallraff *et al.*, Nature (London) **431**, 162 (2004).
[16] R. J. Schoelkopf and S. M. Girvin, Nature (London) **451**, 664 (2008).
[17] J. Koch *et al.*, Phys. Rev. A **76**, 042319 (2007).
[18] E. Jaynes and F. Cummings, Proc. IEEE **51**, 89 (1963).
[19] A. Boca *et al.*, Phys. Rev. Lett. **93**, 233603 (2004).
[20] G. Khitrova, H. M. Gibbs, M. Kira, S. W. Koch, and A. Scherer, Nature Phys. **2**, 81 (2006).
[21] M. Brune *et al.*, Phys. Rev. Lett. **76**, 1800 (1996).
[22] M. Hofheinz *et al.*, Nature (London) **454**, 310 (2008).
[23] I. Schuster *et al.*, Nature Phys. **4**, 382 (2008).
[24] J. M. Fink *et al.*, Nature (London) **454**, 315 (2008).
[25] L. S. Bishop *et al.*, Nature Phys. **5**, 105 (2009).
[26] C. E. López, H. Christ, J. C. Retamal, and E. Solano, Phys. Rev. A **75**, 033818 (2007).
[27] W. Dür, G. Vidal, and J. I. Cirac, Phys. Rev. A **62**, 062314 (2000).
[28] J. K. Stockton, R. van Handel, and H. Mabuchi, Phys. Rev. A **70**, 022106 (2004).
[29] C. E. López, J. C. Retamal, and E. Solano, Phys. Rev. A **76**, 033413 (2007).
[30] T. E. Tessier, I. H. Deutsch, A. Delgado, and I. Fuentes-Guridi, Phys. Rev. A **68**, 062316 (2003).
[31] A. Retzker, E. Solano, and B. Reznik, Phys. Rev. A **75**, 022312 (2007).
[32] D. Leibfried *et al.*, Science **304**, 1476 (2004).